Raman spectra and lattice-dynamical calculations of natrolite

Article *in* European Journal of Mineralogy · May 2001

DOI: 10.1127/0935-1221/2001/0013-0507

2 authors:

Sergei Goryainov
Sobolev Institute of Geology and Mineralogy
171 PUBLICATIONS **1,297** CITATIONS

SEE PROFILE

M. B. Smirnov
Saint Petersburg State University
133 PUBLICATIONS **2,771** CITATIONS

SEE PROFILE

Eur. J. Mineral.
2001, **13**, 507-519

This paper was presented at the EMPG VIII
meeting in Bergamo, Italy (April 2000)

Raman spectra and lattice-dynamical calculations of natrolite

SERGEI V. GORYAINOV[1,*] and MIKHAIL B. SMIRNOV[2]

[1]Institute of Mineralogy and Petrography, pr. Ak.Koptyuga, 3, Novosibirsk, 630090, Russia
[2]Institute for Silicate Chemistry, ul. Odoevskogo, 24, korp.2, St. Petersburg, 199155, Russia

Abstract: Polarized single-crystal Raman scattering and powder infrared absorption spectra of *Fdd*2 orthorhombic natural natrolite $(Na_{1.88}K_{0.02}Ca_{0.04})[Al_{1.96}Si_{3.03}O_{10}]\cdot 2.03\ H_2O$ from Khibiny, Kola peninsula, were measured. Using short-range models, lattice-dynamical calculations were performed for an idealized natrolite structure $Na_4[Al_4Si_6O_{20}]4H_2O$ containing 46 atoms in the primitive unit cell ($Z = 2$). By varying the valence force constants, the calculated frequencies in the Raman and IR spectra were fitted to the observed frequencies. On considering their calculated intensities as well, nearly all the observed bands (especially those corresponding to the A_1 modes) could be unambiguously assigned and interpreted. The external vibrations of H_2O could be correctly assigned using deuterated samples. The strongest Raman band at 534 cm^{-1} corresponds to a breathing mode of the four-membered aluminosilicate ring. The calculated bulk modulus (52.7 GPa at zero pressure) is close to the experimental value of 47 ± 6 GPa.

The natrolite structure has some advantages upon other zeolites to understand the amorphization mechanism, because samples of this mineral surrounded by a non-penetrating medium show no crystal phase transitions with increasing pressure. Lattice energy minimization calculated with variable unit-cell dimensions shows the crystal structure to become unstable at about 5.5 GPa, thereby apparently explaining the amorphization process at 4-7 GPa. This instability is connected with shear acoustic modes coupled with soft internal framework vibrations.

Key-words: Raman spectra, IR spectrum, natrolite, lattice dynamics, vibrational modes, phonon dispersion curves.

1. Introduction

Using lattice dynamics, vibrational frequencies and eigenvectors were calculated for a number of complex aluminium-bearing silicates, including garnets (Patel *et al.*, 1991; Winkler *et al.*, 1991; Pilati *et al.*, 1996; Chaplin *et al.*, 1998), andalusite (Iishi *et al.*, 1979; Salje & Werneke, 1982; Winkler & Buehrer, 1990; Pilati *et al.*, 1997a), beryl (Pilati *et al.*, 1997b), and phlogopite (McKeown *et al.*, 1999). Apart from strict spectroscopic applications, such results are very useful to elucidate vibrationally dependent structural and thermodynamical properties of solids; unfortunately, in view of the more complex structure of zeolites, for these minerals a full set of consistent lattice-dynamical calculations is not available yet in the literature; there only have been attempts to calculate vibrational frequencies using selected unit-cell blocks (Bartsch *et al.*, 1994).

The structure of natrolite $Na_4[Al_4Si_6O_{20}]4H_2O$, which is the simplest one among zeolites (Gottardi & Galli, 1985), can be used as an example of calculation of a full set of vibrational modes and their subsequent comparison with the observed vibrational modes, especially Raman- and IR- active frequencies obtained from a single crystal. The results of such calculations involve the determination of symmetry and relative displacements of all atoms in the modes, including

*E-mail: svg@uiggm.nsc.ru

DOI: 10.1127/0935-1221/2001/0013-0507 0935-1221/01/0013-0507 $ 3.25

the external modes of water molecules in the channels, as well as the evaluation of the elastic moduli and the bulk modulus.

The problem of pressure-induced amorphization of crystals, including the influence of preceding or accompanying solid-phase transformations, is widely studied at present (Gillet *et al.*, 1996; Hemley & Ashcroft, 1998; Ovsyuk & Goryainov, 1999). Since static deformations of crystals connected with variation of thermodynamical parameters can also be considered as frozen vibrations, our calculations can verifiy the instability range of the natrolite structure at high pressure, thereby providing a possibility to elucidate amorphization mechanisms. Note that the natrolite structure has some advantage over other zeolite structures to understand the amorphization mechanisms; such an advantage occurs because only natrolite shows

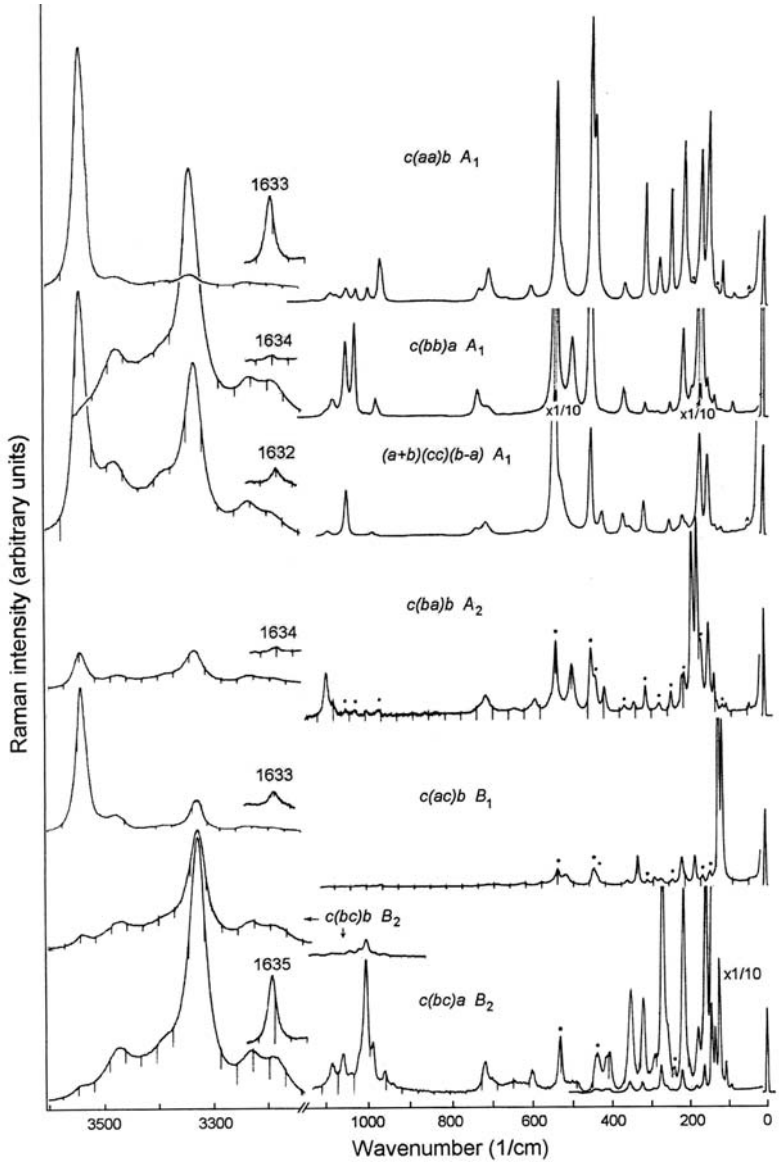

Fig. 1. Raman spectra of single-crystal natrolite using various scattering geometries. The dots mark the remnant bands from other geometry of scattering. The small intensity laser line at 38.4 cm^{-1} is marked by the Λ sign.

no pressure-dependent crystal phase transitions, if compressed in a non-penetrating medium (Kholdeev *et al.*, 1987; Belitsky *et al.*, 1992).

2. Experimental and calculation techniques

Raman spectra of natrolite (Fig. 1) were recorded by a triple DILOR OMARS 89 spectrometer (Goryainov & Belitsky, 1995), equipped by a 1100-channel detector Princeton Inst. LN/CCD-1100 PB and a microscope, as well as by a LOMO DFS-24 spectrometer. A diamond-anvil cell (DAC) was used for high-pressure observations up to 11 GPa at room temperature. Infrared (IR) absorption spectra of powder samples were measured using a Bruker IFS-113v spectrometer: for this purpose, a series of KBr tablets, each of them containing 2 mg of powdered natrolite, were used to obtain data relative to the middle IR region, and polyethylene tablets were used instead for the far IR region.

Natrolite has a narrow-porous structure representing the fifth group of zeolites (Gottardi & Galli, 1985). It has an Al-Si ordered framework, stuffed by exchangeable cations and H_2O molecules. The framework is combined by two parallel chains which are turned by a small angle of about 20° around the ***c***-axis. Both chains are formed by $Si_3Al_2O_{10}$ links oriented in one direction. A (*x,y*)-projection of natrolite unit cell is drawn in Fig. 2 and 3, using Artioli *et al.* (1984) structural data. As a rule, the chemical composition of natural samples from different deposits is close to the ideal formula $Na_2[Al_2Si_3O_{10}]\ 2H_2O$. For polarized Raman measurements, a natrolite single crystal from Khibiny, Kola peninsula, Russia, measuring 5 × 10 × 10-mm^3 along the [110] × [-110] × [001] axes was used, with an additional polished (010) face. The chemical composition of this sample, as determined by electron microprobe analysis, is $(Na_{1.88}\,K_{0.02}\,Ca_{0.04}\,)[Al_{1.96}\,Si_{3.03}\,O_{10}]\ 2.03\ H_2O$. The water content of 9.62 wt.% was measured by TGA as the weight loss during heating to elevated temperatures.

The program LADY (LAttice DYnamics, 1999, by M.B. Smirnov) was used to perform lattice dynamical calculations of natrolite in different approximations, *i.e.* using three different VFF, or

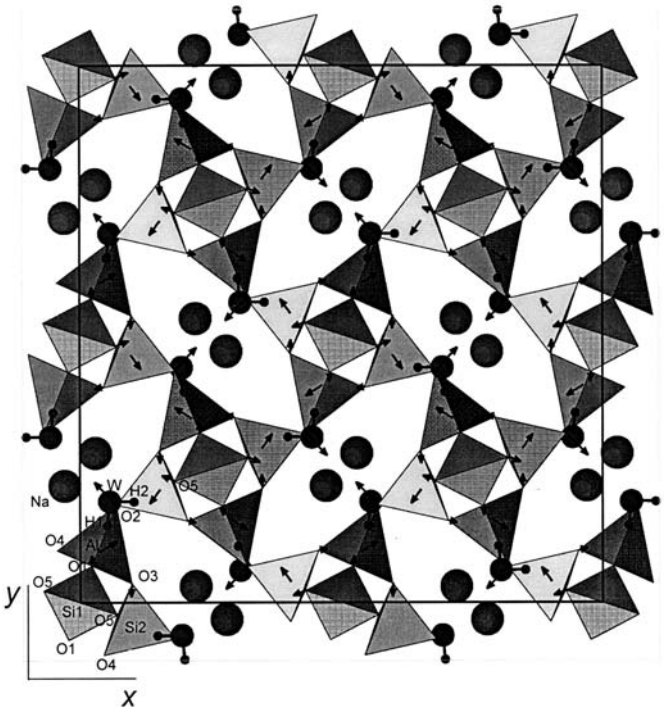

Fig. 2. Vibration form for the strong Raman band of natrolite at 443 cm^{-1}, calculated in the valence force field M-1 model.

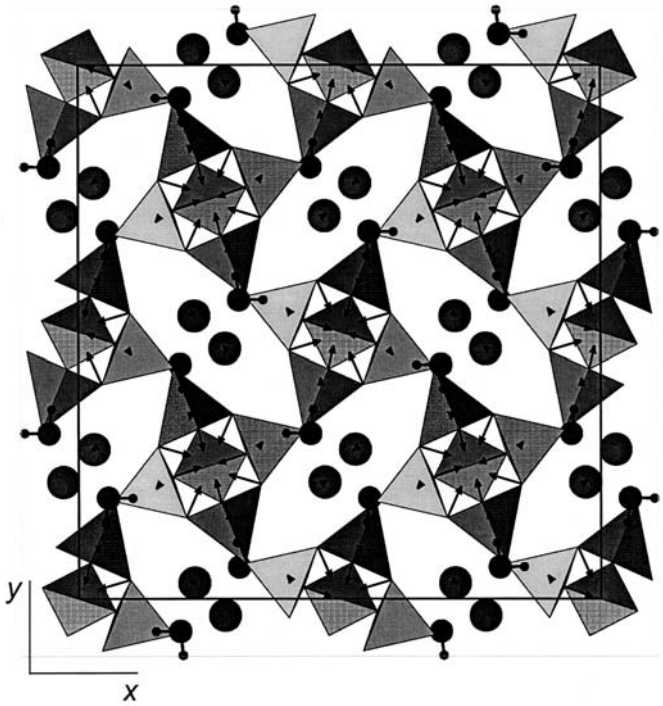

Fig. 3. Vibration form for the strongest Raman band of natrolite at 534 cm^{-1}, calculated in the valence force field M-1 model.

valence force field models (M-1 to M-3), or a set of interatomic potentials (IAP) described by Smirnov *et al.* (1995), respectively. A previous version of this program described by Smirnov *et al.* (1995) was applied to a number of different crystal structures (quartz, zirconia, superconductors, A1N, SiC) and provided results in good agreement with the experimental data (Mirgorodsky *et al.*, 1995, 1999). The IAP model was also used to perform calculations of the crystal structure of natrolite and to estimate its stability with respect to pressure.

3. Results and discussion

3.1 Comparison of calculated and observed Raman spectra of natrolite

Factor group analysis and lattice-dynamical calculations of natrolite vibrations were carried out for the primitive cell of *Fdd*2 space group symmetry, Z = 2, containing 46 atoms: $Na_4[Al_4Si_6O_{20}]$ $4H_2O$. According to theory, there should be a total of 99 optically active modes $24A_1 + 25A_2 + 25B_1 + 25B_2$ concerning motion of framework and intrachannel cations, to be compared with a total of 78 peaks observed in Raman and IR spectra ($28A_1 + 15A_2 + 12B_1 + 23B_2$), and a few additional modes discussed below (Tables 1 and 2, Fig. 1). All the Raman bands below 1100 cm^{-1} are quite narrow with a bandwidth of about 5-7 cm^{-1}. Of the predicted total of 74 IR-active modes (not concerning water vibrations), 36 peaks only were observed in the IR spectra, and of the predicted 36 optically-active (Raman and IR) modes $9A_1 + 9A_2 + 9B_1 + 9B_2$ implying water molecules, only 16 main modes $7A_1 + 3A_2 + 3B_1 + 3B_2$ were reliably observed. In addition, 16 O-H vibrational peaks ($4A_1 + 4A_2 + 4B_1 + 4B_2$) could be detected. Several external modes of H_2O seem to be overlapped by strong framework bands (Tables 1-3). Using light-scattering geometry (Fig. 1, Table 1) the appropriate symmetry and TO-LO labelling could be assigned to the different modes. Some purely transverse optical (TO) modes are marked in Table 1, whereas the other modes belong to mixed longitudinal-transverse optical LO-TO type. Additional peaks (including A_1 modes at 520, 976 and 1072 cm^{-1}) appear to be due to the effect of longitudinal-transverse interaction on phonon frequen-

Table 1. Observed Raman band frequencies (cm^{-1}) for different scattering geometry of single crystal natrolite and IR spectrum of powder natrolite.

A_1 TO $b'(cc)a'$	A_1 $c(bb)a$	A_1 $c(aa)b$	A_2 $c(ba)b$	B_1 TO $c(ac)b$	B_2 $c(bc)b$	B_2 TO $c(bc)a$	A_1 B_1 B_2 IR
75	76	75	99		93	93	75, 90
104		106		115	106	106	105, 112
123	124		129	121	123	123	122
140	142	141	141		135	135	134,143
160	160	160	170		162	162	162
187			184	182	183	183	183, 197
206		206	211	216	221	222	205, 219
242		242					240
		272		273	276	277	263, 277
				289	297	297	290
308	307	307					
345			336	331	329	326	326, 347
361	360	360		358	360	358	361
414			413		415	415	418
		434					
443	443	444					442
518	492	522	495	514	496	495	487, 510
534	534	534					542
599			598	588	576	604	575, 602
		657^{vs}	633	619			623, 648^{sh}, 677
704	703	703	708				
728	727	725			723	722	720
965		965		967	965	964	967
978	973						982
		993	996		988	993	999
	1025	1024			1009	1009	
1040	1046	1047			1026		1040
	1076	1071	1075		1047	1063	1061
1083	1089	1083	1092			1088	1090
1632	1634	1633	1634	1633	1635	1635	1635
3189	3186	3187	3190	3183	3183	3184	3187
3225	3227	3226	3227	3228	3227	3229	3224
3331	3331	3331	3330	3330	3329	3328	3328
3384	3386	3384	3385	3386	3385	3385	3391
3475	3473	3473	3472	3471	3471	3472	3461
3543		3542	3542	3542	3541	3543	3539

Remarks. $b'=b-a$, $a'=a+b$, TO is transverse phonon. ^{vs} is very small intensity. ^{sh} is the shoulder of the band.

cy; such a phenomenon is similar to the dependence of Si-O vibration frequency upon the wave vector direction, which has been observed in quartz (Wilkinson, 1973).

For each mode, the calculated main amplitudes of motion for the atoms are shown in Tables 2 and 3. It appears that all atoms can participate in almost every vibrational mode.

Intensities of (*aa*), (*bb*) and (*cc*) polarization spectra in Fig. 1 essentially differ, thereby proving the existence of strong anisotropy in bond polarizability. In our calculations of the intensity of Raman peaks, we assumed longitudinal polarizability of T-O bonds; the calculated intensities are in satisfactory agreement with the experimental values. Such results suggest that the Si1-O-Si2 bonds making an angle of about 20° with the ***a***-axis are essentially covalent and give a strong contribution to the intensity of the Raman bands, whereas the Sil-O-Al bonds elongated along the ***b***-axis are essentially ionic and result in a smaller intensity of the bands. The polarization of the Si2-O-Al bonds gives equal contributions in all (*aa*), (*bb*) and (*cc*) polarization spectra.

Table 2. Assignment of the fully symmetric (A_1) vibrational modes of natrolite framework and intrachannel cations by comparison of the observed frequencies with our calculated values using the M-2 model.

Framework and intrachannel cation vibrations.

Freq. (cm^{-1}) Exper.	Calc. M-2	Intensity Exper.	Calc. M-2	Main amplitudes (10^{-2}) M-2	Vibration type
75	72	0.02	0.004	9Na+4W	tr_zNa
105	102	0.15	0.05	8Na+3O1+2O2+4O3+4O4+3O5+2H1+2H2	tr_{xy}Na
123	115	0.05	0.09	3Na+2Si2+2Al+6O1+3O3+3O4+6O5+5W+4H1+7H2	twist $Si_3Al_2O_{10}$ link
141	142	0.63	0.02	5Na+2Si2+2Al+5O3+4O4+8W+4H1+3H2	distort $Si_2Al_2O_{10}$ ring+ tr_{yx}W+tr_zNa
160	167	0.63	0.23	5Na+3Si2+4Al+4O2+4O3+5O4+4W+5H1+2H2	$tr_{xy}AlO_4$+tr_yNa
206	197	0.3	0.07	6Na+2Si1+4Si2+3Al+3O2+4O3+4O4+2O5+3W+2H1	tr_{xyz}Na
242	214	0.2	0.12	4Na+4Si2+5Al+4O2+3O3+5O4+2H1+3H2	$tr_{xy}Si2O_4$+$tr_{xy}AlO_4$+tr Na
272*	-	0.08	-		
307	307	0.26	0.07	3Si1+3Al+2O1+8O2+6O3+5O4+4O5+2H1+2H2	lib TO_4
345	344	0.02	0.17	3Si2+4Al+6O1+6O2+4O3+4O4+4O5+4H1+7H2	lib TO_4
360	358	0.06	0.03	2Si2+3Al+8O1+3O2+5O3+5O4+2O5+7H1+6H2	lib TO_4
414	395	0.04	0.29	3Si1+3Si2+5Al+3O1+5O2+3O3+4O5+15H1+16H2	lib TO_4+tr_xAlO_4+lib_zH_2O
434	413	0.64	0.05	5Si1+3Si2+2O1+5O2+5O3+6O4+4O5+7H1+8H2	O-T-O bend AlO_4+lib TO_4
443	446	0.8-	0.08	6O1+3O3+3O4+9O5+10H1+10H2	O-T-O bend $Si1O_4$
492	500	0.2	0.29	6Si1+2Si2+2Al+5O1+3O3+3O4+5O5+2W+16H1+16H2	O-T-O bend+$lib_{xy}H_2O$
520*	-	0.2	-		
534	535	1.02	1.02	6O1+7O3+7O4+6O5+2H1	O-T-O bend breath
599	603	0.1-	0.18	3Si1+2Si2+5Al+6O1+2O2+3O3+3O4+2O5+5H1+20H2	O-T-O bend AlO_4,$Si1O_4$
657	649	0.01	0.34	4Si1+5Si2+4Al+2O1+5O2+3O4+6O5+5H1+14H2	O-T-O bend TO_4
703	667	0.06	0.4	2Si1+5Si2+6Al+4O2+5O3+2O4+4O5+3H1+9H2	O-T-O bend AlO_4, $Si2O_4$
727	687	0.1	0.37	5Si2+5Al+6O2+3O3+5O4+2O5+8H1+2H2	O-T-O bend AlO_4, $Si2O_4$
965	976	0.19	0.94	3Si2+2Al+6O2+5O3+8O4+2O5	T-O stretch TO_4
976*	-	0.03	-		
993	988	0.05	0.62	4Si1+3Al+11O1+2O5	T-O stretch $Si1O_4$, AlO_4
1025	1011	0.15	0.46	5Si2+2Al+8O2+2O3+6O4	T-O stretch $Si2O_4$, AlO_4
1040	1028	0.15	0.48	5Si2+2Al+4O2+9O3+2O4	T-O stretch $Si2O_4$
1072*	-	0.01	-		
1083	1083	0.03	0.45	4Si1+4Si2+11O5	T-O stretch. $Si1O_4$, $Si2O_4$

Remarks. * are observed modes, additional to the modes predicted by LD calculations. W is O atom of H_2O molecule.

Raman modes are given with frequencies and integral intensities, which are mean values for different scattering geometries presented in Table 1.Vibration type is marked by : tr-translation with main amplitudes along the directions *x,y,z*, lib-libration, bend-bending, stretch-stretching, twist-twisting of $Si1Si2_2Al_2O_{10}$ link and distort- square-rhombic distortion of $Si2_2Al_2O_{10}$ ring.

3.2 Vibrations of water molecules in natrolite

The Raman frequencies of D_2O-natrolite were calculated (see Table 3) using the M-2 model with the same valence force constants as for H_2O-natrolite and also using the M-3 model, which uses essentially different valence force constants (Table 4). These data prove that molecular geometry and hydrogen bonds differ in H_2O- and D_2O-natrolites.

There is a remarkable agreement between the polarization of Raman spectra involving O-H (O-D) stretching vibrations and the calculated intensity. Fig. 1 shows that in the (*a,b*)-plane the 3542-cm^{-1} band is almost completely (*aa*)-polarized along the ***a***-axis, whereas the 3331-cm^{-1} band is almost completely (*bb*)-polarized along the ***b***-axis. This polarization is explained by orientation of the bonds and localization of stretching vibrations in one of two O-H bonds with corresponding alternative amplitudes of H2 or H1 atoms, as it is shown in Table 3, due to strongly different force constants (Table 4). Viewing natrolite in the (*a,b*)-plane (Fig. 2) shows that O-H1 bond is nearly parallel to the ***b***-axis, whereas O-H2 bond is nearly parallel to the ***a***-axis.

The Raman spectrum of water in natural natrolite in Fig. 1 exhibits two main O-H bands at ν_1 = 3331 cm^{-1} and ν_3 = 3542 cm^{-1} and several additional bands of smaller intensity, which can be combined in two doublets at ν'_1 = 3187, ν'_3 =

Table 3. Assignment of the fully symmetric (A_1) vibrational modes of water molecules in natrolite, using the M-2 and M-3 models.

Vibrations of H_2O molecules in natural natrolite.

Freq. (cm^{-1}) Exper.	Calc. M-2	Intensity Exper.	Calc. M-2	Main amplitudes (10^{-2}) Calc. M-2	Vibration type
143^{IR}	148	-	0.03	5Na+3Si2+4O3+3O4+2O5+9W+2H1+8H2	$tr_{yx}H_2O$
-	155	-	0.05	2Na+2Al+2O1+2O3+2O4+2O5+10W+9H1+11H2	$tr_{xy}H_2O$
187	179	0.04	0.06	2Na+2Al+2O1+2O3+2O4+11W+11H1+9H2	tr_zH_2O
(412)	393	-	0.21	2Si1+3Si2+4O1+5O2+3O4+3O5+2W+22H1+23H2	lib_zH_2O (tr_xH1,tr_yH2)
-	612	-	0.23	3Si1+2Si2+3Al+3O1+2O3+2O5+42H2	$lib_{xy}H_2O$ (tr_zH2)
706	704	0.08	0.06	2O2+2O4+48H1+5H2	$lib_{xy}H_2O$ (tr_zH1)
1633	1632	0.3	0.19	3W+35H1+33H2	H-O-H bend
3331	3332	1.2	1.68	3W+47H1+13H2	O-H stretch (tr_yH1)
3542	3542	1.5	1.65	3W+12H1+47H2	O-H stretch (tr_xH2)

Vibrations of D_2O molecules in D_2O-natrolite.

Freq. (cm^{-1}) Exper.	Calc. M-2	M-3	Intensity Exper.	Calc. M-3	Main amplitudes (10^{-2}) Calc. M-3	Vibration type
135^{IR}	145	145	-	0.03	5Na+3Si2+4O3+4O4+3O5+7W+10D2	$tr_{yx}D_2O$
-	150	150	-	0.05	4Na+3O1+4O3+3O4+2O5+9W+9D1+6D2	$tr_{xy}D_2O$
(175)	173	173	-	0.06	3Na+3Al+3O2+3O3+3O4+9W+10D1+8D2	tr_zD_2O
(303)	295	296	-	0.21	2Si1+3Si2+2O1+3O2+4O3+2O4+4W+20D1+20D2	lib_zD_2O (tr_xD1,tr_yD2)
-	453	453	-	0.23	3Si1+4O2+4O3+3O5+28D2	$lib_{xy}D_2O$ (tr_zD2)
502	516	517	0.07	0.06	4O1+2O2+3O3+5O4+2O5+28D1+5D2	$lib_{xy}D_2O$ (tr_zD1)
673*			0.06			
1199	1195	1200	0.3	0.18	4W+24D1+22D2	D-O-D bend
2472	2411	2472	1.5	1.65	3W+31D1+13D2	O-D stretch (tr_yD1)
3632	2571	3634	0.8	1.53	3W+12D1+31D2	O-D stretch (tr_xD2)

Remarks. The suggested non-resolved bands (under framework bands) are shown in parenthesis. ^{IR} is the band from infrared spectrum. * is an additional observed mode. W is O atom of water molecule.

Vibration type is marked by tr-translation with main amplitudes along the directions *x,y,z*, lib-libration, bend-bending, stretch-stretching.

3385 and ν''_1 = 3226, ν''_3 = 3473 cm^{-1}. These two doublets can be ascribed to vibration of H_2O molecules located in two additional sites in the crystal, W' and W'', with approximate relative occupancy of about 5 % with respect to that of the main W site, which is almost completely occupied. This assumption is supported by the chemical composition of natural natrolite, which shows an excess of water of at least 1.5 % (or 0.03 H_2O per ideal 2 H_2O formula unit).

The frequencies of internal vibrations with different symmetry practically coincide, thereby suggesting the absence of strong water-water interaction. The small bandwidth (25-35 cm^{-1}) of internal H_2O vibrations (vibrons) is in favour of proton ordering in all positions of water in natrolite. Note that there are different contributions in the broadening of bands. For instance, the increase of the vibron bandwidth at phase transition from ice VIII to ice VII at high pressure has been tentatively assigned to its decay into bending modes (Besson *et al.*, 1997).

The external vibrations of water molecules in natrolite are given in Table 3. Reliably observed bands of this kind occur at 706 and 187 cm^{-1} or at 143 cm^{-1} in the Raman or IR spectrum, respectively, and are essentially shifted on deuteration. In the Raman spectrum these bands have low intensity, and are slightly broader than the other bands. The Raman bands at 502 and 673 cm^{-1} proper to D_2O-natrolite are well distinguished. The latter one cannot belong to a D_2O libration mode, and should rather be ascribed to a framework mode with intensity enhanced due to interaction with heavy water. Several external H_2O vibration bands were not distinguished, very probably because they are overlapped by strong framework bands. Moreover, there are several additional framework modes which strongly interact with external water modes, and this situation leads to large frequency

Table 4. Force constants in valence force field M-2 and M-3 models, used for calculation of natrolite vibrations in Tables 2 and 3.

bond, angle	angle/ same angle (mdyn·Å)	angle/ bond (mdyn)	angle/ neighbour angle (mdyn·Å)	bond/ neighbour bond (mdyn/Å)
Si-O, O-Si-O	0.98	0.25	0.18	0.33
Al-O, O-Al-O	0.55	0.17	0.11	0.21
O-T, T-O-T	0.056	0	0	0
W-H, H-W-H	0.580	0.235	0	-0.1
W-D, D-W-D	0.582	0.235	0	-0.1

bond	bond/same bond (mdyn/Å)	*R*1 (Å)	*R*2 (Å)
Al-O	3.3	1.708	1.720
Si1-O1	4.8	1.630	
Si1-O5	4.8	1.642	
Si2-O2	5.15	1.641	
Si2-O3	5.15	1.638	
Si2-O4	4.8	1.635	
Si2-O5	4.8	1.647	
W-H1	6.05	0.878	
W-H2	6.75	0.933	
W-D1	6.37	0.878*	
W-D2	7.0	0.933*	
O-O	0.08	2.85	3.0
O-O	0.06	3.0	3.1
O-O	0.03	3.1	3.2
O-O	0.02	3.2	3.6
Na-O	0.17	0	3.0
Na-W	0.05	0	2.9
W-O	0.045	0	3.5
H-O	0.11	1.5	2.5
H-O	0.087	2.5	3.5
D-O	0.11	1.5	2.5
D-O	0.087	2.5	3.5

Remarks. *structural parameters of D_2O-natrolite were taken the same as that of H_2O-natrolite.

shifts on deuteration, for instance, the H_2O-natrolite framework mode at 414 cm^{-1} shifts in D_2O-natrolite to 396 cm^{-1}. The observation of external vibrations of water for zeolites allows to elucidate essential features of hydrogen bonds and water-cation interaction. Although such a feature is especially characteristic for zeolites, a similar situation concerning such modes occurs in natrolite and gypsum (Berenblut *et al.*, 1971). At low temperatures, apparent bands of external vibrations of water molecules in proton-ordered ices were recorded (Sherman & Wilkinson, 1980). In liquid water at ambient conditions, a translational modes were observed in Raman spectra at 50 and 170 cm^{-1} (Moskovits & Michaelian, 1978), which are essentially lower than corresponding vibrations in natrolite (Table 3). In liquid water there is a translational mode at 290 cm^{-1}, which can be interpreted as the W-W motion, leading to high frequency due to the small effective mass (coefficient 1/2). Such motions are impossible in natrolite, where each water molecule is isolated and there is no water-water interaction. Note that the libration modes of H_2O in dioptase were observed at 613 and 732 cm^{-1} (Goryainov, 1996); such values are close to the corresponding modes in natrolite (Table 3).

In comparison with the Raman spectra reported by Pechar *et al.* (1981), we observed about 40 additional bands involving framework and extra-framework cations in different scattering geometry, which can be related to 27 modes. Since the intensity of many bands reported by these authors is essentially different from our results, a first possible explanation could be that the crystals used come from different localities and are physically different; however, their compositions are close to that of the ideal formula. Therefore, we have good reasons for assuming that there are mistakes in the table of Raman intensities given by Pechar *et al.* (1981). The frequencies of many corresponding bands also significantly differ, as for instance our

(*bb*) peak at 492 cm^{-1} versus 480-482 cm^{-1}, or our 3331 cm^{-1} versus 3293 cm^{-1} of Pechar *et al.* (1981). The good accuracy of our wavelength measurements obtained from neon-line lamp calibration is confirmed by the frequency coincidence of the corresponding bands in different geometry of Raman scattering, as well as by the vicinity of Raman and IR frequencies of several bands, including the O-H stretching bands.

3.3 Parameters of the valence force field models

As it was stated before, our calculations of vibrational spectra were performed using a number of VFF (M-1, M-2, M-3) and IAP models. In the VFF M-1 and IAP models the water molecule H_2O was represented as effective atom. The details of the parameter fitting in different models are discussed below, while the results of the M-1 model are given in Fig. 2 to 4. The forms of two modes, most intensive in Raman spectra, calculated in the M-1 model are represented in Fig. 2 and 3.

Fig. 4 exhibits the phonon dispersion curves of natrolite along ***c*** all over the Brillouin zone calculated in the M-1 model. The dispersion curves in the ranges of 20-350 and 650-700 cm^{-1} exhibit the maximum steepness. Several branches in the range of 940-990 cm^{-1} have also significant slopes, whereas other curves are much flatter, and this effect is probably due to the localized motion of oxygen atoms.

The parameters in VFF models (M-1, M-2, M-3) were adjusted on the basis of best fit of the calculated frequencies to the corresponding experimental values, and as a result the set of force constants was obtained and reported in Table 4. For instance, the force constant *K*(Si-O) varies from 4.8 to 5.15 mdyn/Å for different Si-O bonds. These values of *K*(Si-O) fitted in the model are not connected with Si-O bond length, which changes very little in natrolite, but they express the effective influence of surrounding atoms. Other force constants are given a unique value for each kind of bonds (Al-O) and angles.

For the M-1 model the diagonal force constants are *K*(Al-O) = 3.2 mdyn/Å, *K*(O-Si-O) = 0.89 mdyn·Å, *K*(O-Al-O) = 0.55 mdyn·Å, *K*(T-O-T) = 0.28 mdyn·Å, where T = Al, Sil, Si2. Cation-framework interactions are expressed in terms of force constants *K*(Na-O) = 0.2 mdyn/Å at distances up to 3 Å. Always in this M-1 model, the interaction of water with the coordination polyhedra involves the force constants *K*(W-Na) = 0.1 mdyn/Å and *K*(W-O) = 0.15 mdyn/Å, where W is the oxygen atom of the water molecule.

Three VFF models also involve a long-distance intertetrahedral interaction expressed in the decreasing sequence of force O-O constants, given in Table 4. This stepwise approximation is based on the calculated dependence of O-O force constant on distance (Mirgorodsky *et al.*, 1999). Such long-distance O-O interaction plays an essential role in reproducing the experimental bulk modulus value of quartz (Lazarev & Mirgorodsky, 1991). Note that in the case of natrolite the crystal stiffness increase with respect to quartz is essentially due to Na-O interaction, and as a result the intertetrahedral O-O interaction plays a minor role.

In the M-2 model with H_2O as water molecule (while in the M-1 model H_2O was considered as effective atom), we found that several force constants in the optimized set of parameters are notably different from those in the M-1 model. For instance: *K*(T-O-T) = 0.056 mdyn·Å, *K*(Na-O) = 0.17 mdyn/Å, *K*(W-Na) = 0.05 mdyn/Å, *K*(W-O) = 0.045 mdyn/Å, *K*(O-H1) = 0.11 mdyn/Å, *K*(O-

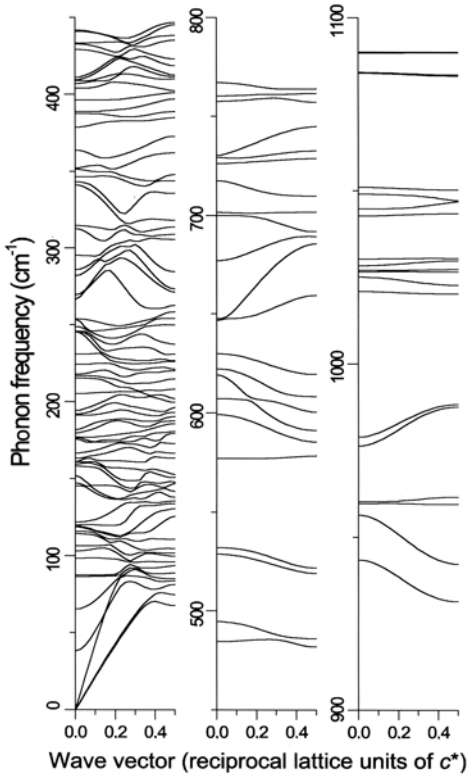

Fig. 4. Phonon dispersion curves for natrolite along ***k***(00ξ), calculated using the valence force field M-1 model.

H2) = 0.087 mdyn/Å, K(W-H1) = 6.05 mdyn/Å, K(W-H2) = 6.75 mdyn/Å, K(H1-W-H2) = 0.58 mdyn·Å.

In Table 3, together with the corresponding experimental values, the calculated vibrational frequencies of D_2O-natrolite are reported, where the same force constants as in the M-2 model have been used. In addition, those obtained from the M-3 model are also reported: here, the internal force constants for the water molecule are higher: K(W-D1) = 6.67 mdyn/Å, K(W-D2) = 7.0 mdyn/Å, K(D1-W-D2) = 0.582 mdyn·Å.

3.4 Calculation of elactic moduli. Measured and calculated bulk modulus

The value of the bulk modulus K_0 = 52.7 GPa calculated in the M-2 model is close to the corresponding experimental value K_0 = 47 ± 6 GPa, which was obtained from treatment of our X-ray diffraction data in DAC (Kholdeev *et al.*, 1987) (Fig. 5). Note that the bulk modulus in quartz is 37.1 GPa, and that in coesite is 96 GPa (Kuskov & Fabrichnaya, 1987). Elastic moduli of natrolite at zero pressure calculated in the M-2 model are equal (in GPa) to: C_{11} = 82.2, C_{22} = 78.5, C_{33} = 146.6, C_{44} = 34, C_{55} = 38.2, C_{66} = 31.9, C_{12} = 30.3, C_{13} = 39.5, C_{23} = 34.9.

3.5 Localised Raman modes in natrolite and glasses

According to some authors (Pasquarello & Car, 1998; Sykes & Kubicki, 1996), silicate glasses exhibit two sharp peaks at 495 and 606 cm^{-1} in the Raman spectrum, which correspond to breathing vibrations of four- and three-membered rings. Frameworks of zeolites contain different four-membered rings: therefore, using zeolite structures a correlation between the frequency of strong breathing modes and the geometry of four-membered rings can be obtained. For these reasons, the present assignment of the observed vibrational modes of natrolite is the first step to establish this correlation in terms of composition and form of four-membered rings, a point which would be precious to elucidate the internal structure of glasses. For instance, the strongest Raman band at 534 cm^{-1} in natrolite corresponds to the breathing mode in the so-called «double-covered» four-membered ring with internal circle -Al-O3-Si2-O4-Al-O3-Si2-O4- (see Fig. 3), which is covered from above and below by two $Si1O_4$ tetrahedra; instead, a similar peak ascribable to such a breathing mode in double-covered four-membered rings has not been observed in Raman spectra of glasses (Pasquarello & Car, 1998). For such non-crys-

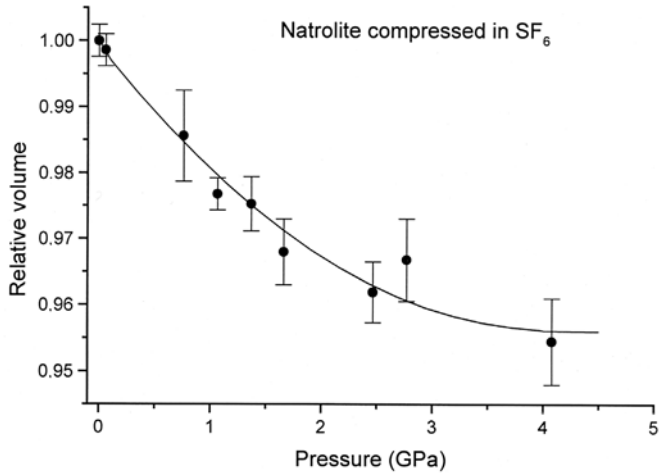

Fig. 5. Pressure dependence of the unit-cell volume of natrolite compressed in SF_6. Experimental values (Kholdeev *et al.*, 1987) obtained by X-ray measurements in DAC are shown by solid circles. The calculated curve corresponds to a polynomial fit to experimental points by least squares (up to the third power in P); from this interpolation the bulk modulus K_0 = 47 ± 6 GPa and its derivative K_0' = 5.8 ± 0.8 were obtained.

talline materials, the main peak at 495 cm^{-1} corresponds to simple («non-covered») four-membered rings, and such result agrees with calculations (Sykes & Kubicki, 1996). This peak is very close to the strongest peak at about 500 cm^{-1} in analcime (Goryainov *et al.*, 1996), a peak which rather belongs to the breathing mode in simple four-membered rings.

The Raman spectrum of natrolite exhibits a second intensive band at 443 cm^{-1}, which corresponds to a localized O2 oxygen bridge mode (Fig. 2). This mode may be also interpreted as a collapse mode of the helical eight-membered ring forming the channel along [001] or as a non-symmetric breathing mode of the closed eight-membered rings forming the channels along [110]. The origin of the strong 430-cm^{-1} peak D_1' in glasses is discussed in Pasquarello & Car (1998), or also in Sykes & Kubicki (1996). Our reasonably grounded assignment of strong bands at 434 and 443 cm^{-1} in natrolite (Table 2), which are close to the D_1' peak, as it is obtained from lattice dynamics, should elucidate the nature of the glass peak: we suggest that it is a breathing mode of eight-membered ring, presumably involving the motion of the four O atoms inside the ring.

3.6 Interatomic potential model calculation of pressure-induced instability of natrolite

Lattice energy minimization using interatomic potentials was also performed in the IAP model for a set of variable unit-cell parameters, in order to predict thermodynamical behaviour of natrolite with respect to pressure. To describe the long-range interaction, the electrostatic or coulombic term is used

$$U_C = \Sigma_{ij}\, e^2\, q_i\, q_j\, /r_{ij},$$

where e is the electron charge, q_i and q_j are numbers of effective point charges of i and j ions, and r_{ij} is the distance between them. Taking into account the short-range repulsive forces and the attractive dispersion dipole-dipole forces, Buckingham potential is used

$$U_B = \Sigma_{ij}\, A_{ij} \exp(-r_{ij}/B_{ij}) + C_{ij}/r_{ij}^{Dij},$$

where all $D_{ij} = D = 6$. For Na-O, Si-O, Al-O and O-O interatomic interaction the potential $U = U_B + U_C$ is used.

For Na-W, W-O interatomic interaction the Born-Karman potential with constants $E_{ij} = d^2U/dr_{ij}^2$, $F_{ij} = (1/r_{ij})dU/dr_{ij}$ is used in Table 5 (Smirnov *et al.*, 1995).

According to the calculations in the IAP model, natrolite should become unstable at about 5.5 GPa. This instability seems to correspond to the amorphization in the pressure range of 4-7 GPa observed using polarized microscopy. This instability is shown by the presence of shear acoustic modes coupled with soft internal framework vibrations having B_2 symmetry at $\boldsymbol{k} = 0$. These coupled internal modes correspond to displacement of $Si1O_4$ tetrahedra perpendicular to the C_2 axis and involve distortions of all tetrahedra, especially the AlO_4. Moreover, the framework instability is enhanced by the large displacements of the H_2O molecules from their initial sites occurring at high pressure.

4. Concluding remarks

As a conclusion, the present almost complete assignment of the polarized Raman and IR spectra of natrolite using lattice dynamics can be the basis for interpreting the vibrational spectra of other

Table 5. Parameters A_{ij}, B_{ij}, C_{ij}, D, E_{ij}, F_{ij}, q_i of interatomic Buckingham, Born-Karman and Coulomb potentials used in IAP model for calculation of pressure dependence of natrolite structure stability.

Atom pair	A_{ij} (mdyn·Å)	B_{ij} (Å)	C_{ij} (mdyn·Å^{D+1})	D	$R1$(Å)	$R2$(Å)
Si-O	$2.881 \cdot 10^3$	0.2052	-21.3	6	0	20
Al-O	$2.561 \cdot 10^3$	0.2085	-20.89	6	0	20
O-O	$0.222 \cdot 10^3$	0.3623	-28.0	6	0	20
Na-O	$0.934 \cdot 10^3$	0.2387	0	0	0	20
Atom pair	E_{ij} (mdyn/Å)	F_{ij} (mdyn/Å)			$R1$(Å)	$R2$(Å)
Na-W	0.2	0.02			0	3
W-O	0.05	0.01			0	3
Charge	Na	Al	Si	O	W	$R1$(Å)	$R2$(Å)
q_i	1	1.4	2.4	-1.2	0	0	∞

$R1$ and $R2$ are radii of interaction limits for calculations.

zeolites; these results can also be precious to explain many thermodynamic properties of these minerals, including their behaviour at high pressure.

Acknowledgements: We thank I.A. Belitsky, Yu.V. Seryotkin and G.P. Valueva for fruitful discussions. This work benefited greatly from constructive reviews by C. Gramaccioli and B. Kolesov. This work was supported by the Russian Academy of Sciences, the Russian Foundation for Basic Researches (98-05-65658 and 00-05-65305 grants) and Educational Scientific Centre (NSU-UIGGM). The research described in this publication was made possible in part by Award No. REC-008 of the U.S. Civilian Research & Development Foundation for the Independent States of the Former Soviet Union (CRDF).

References

Artioli, G., Smith, J.V., Kvick, A. (1984): A neutron diffraction of natrolite $Na_2Al_2Si_3O_{10}$ $2H_2O$ at 20 K. *Acta Cryst.*, **C40**, 1658-1662.

Bartsch, M., Bornhauser, P., Calzaferri, G., Imhof, R. (1994): $H_8Si_8O_{12}$: A model for the vibrational structure of zeolite-A. *J. Phys. Chem.*, **98**, 2817-2831.

Belitsky, I.A., Fursenko, B.A., Gabuda, S.P., Kholdeev, O.V., Seryotkin, Yu.V. (1992): Structural transformation in natrolite and edingtonite. *Phys. Chem. Minerals*, **18**, 497-505.

Berenblut, B.J., Dawson, P., Wilkinson, G.R. (1971): The Raman spectrum of gypsum. *Spectrochim. Acta*, **27A**, 1849-1863.

Besson, J.M, Kobayashi, M., Nakai, T., Endo, S., Pruzan, Ph. (1997): Pressure dependence of Raman linewidths in ices VII and VIII. *Phys. Rev. B*, **55**, 11191-11201.

Chaplin, T., Price, G.D., Ross, N.L. (1998): Computer simulation of the infrared and Raman activity of pyrope garnet, and assignment of calculated modes to specific atomic motions. *Am. Mineral.*, **83**, 841-847.

Gillet, P., Malézieux, J.-M., Itié, J.-P. (1996): Phase changes and amorphization of zeolites at high pressures: The case of scolecite and mesolite. *Am. Mineral.*, **81**, 651-657.

Goryainov, S.V. (1996): Dehydration-induced changes in the vibrational states of dioptase $Cu_6Si_6O_{18}$ $6H_2O$. *J. Structural Chem.*, **37**, 58-64.

Goryainov, S.V. & Belitsky, I.A. (1995): Raman spectroscopy of water tracer diffusion in zeolite single crystals. *Phys. Chem. Minerals*, **22**, 443-452.

Goryainov, S.V., Fursenko, B.A., Belitsky, I.A. (1996): Phase transitions in analcime and wairakite at low-high temperatures and high pressure. *Phys. Chem. Minerals*, **23**, 297-298.

Gottardi, G. & Galli, E. (1985): Natural zeolites. Springer-Verlag, Berlin Heidelberg New York.

Hemley, R.J. & Ashcroft, N.W. (1998): The revealing role of pressure in the condensed matter sciences. *Phys. Today*, **51**, 26-32.

Iishi, K., Salje, E., Werneke, C. (1979): Phonon spectra and rigid-ion model calculations on andalusite. *Phys. Chem. Minerals*, **4**, 173-188.

Kholdeev, O.V., Belitsky, I.A., Fursenko, B.A., Goryainov, S.V. (1987): Structural phase transformations in natrolite at high pressures. *Doklady Akademii Nauk*, **297**(4), 946-950 (in Russian). Translated in: *Doklady Earth Sciences*, 1987, 297.

Kuskov, O.L. & Fabrichnaya, O.B. (1987): The SiO_2 polymorphs: the equations of state and thermodynamic properties of phase transformations. *Phys. Chem. Minerals*, **14**, 58-66.

Lazarev, A.N. & Mirgorodsky, A.P. (1991): Molecular force constants in dynamical model of α-quartz. A calculation of phonon spectrum, elastic and piezoelectric properties. *Phys. Chem. Minerals*, **18**, 231-243.

McKeown, D.A., Bell, M.I., Etz, E.S. (1999): Raman spectra and vibrational analysis of the trioctahedral mica phogopite. *Am. Mineral.*, **84**, 970-976.

Mirgorodsky, A.P., Smirnov, M.B., Abdelmounim, E., Merle, T., Quintard, P.E. (1995): Molecular approach to the modelling of elasticity and piezoelectricity of SiC polytypes. *Phys. Rev. B*, **52**, 3993-4000.

Mirgorodsky, A.P., Smirnov, M.B., Quintard, P.E. (1999): Phonon spectra evolution and soft-mode instabilities of zirconia during the c-t-m transformation. *J. Phys. Chem. Solids*, **60**, 985-992.

Moskovits, M. & Michaelian, K.H. (1978): A reinvestigation of the Raman spectrum of water. *J. Chem. Phys.*, **69**, 2306-2311.

Ovsyuk, N.N. & Goryainov, S.V. (1999): High-pressure twisting of tetrahedra and amorphization in α-quartz. *Phys. Rev. B*, **60**, 14481-14484.

Pasquarello, A. & Car, R. (1998): Identification of Raman defect lines as signatures of ring structures in vitreous silica. *Phys. Rev. Lett.*, **23**, 5145-5147.

Patel, A., Price, G.D., Mendelssohn, M.J. (1991): A computer simulation approach to modelling the structure, thermodynamics and oxygen isotope equilibria of silicates. *Phys. Chem. Minerals*, **17**, 690-699.

Pechar, F., Gregora, I., Rykl, D. (1981): Laser Raman polarisation spectra of natural zeolite -natrolite. Coll. Czechoslovak. *Chem. Commun.*, **46**, 3043-3048.

Pilati, T., Demartin, F., Gramaccioli, C.M. (1996): Atomic displacement parameters for garnets: A lattice-dynamical evaluation. *Acta Cryst.*, **B52**, 239-250.

—, —, — (1997a): Transferability of empirical force fields in silicates: Lattice-dynamical evaluation of atomic displacement parameters and thermodynamic properties for the Al_2SiO_4 polymorphs. *Acta Cryst.*, **B53**, 82-94.

—, —, — (1997b): Lattice-dynamical evaluation of thermodynamic properties and atomic displacement parameters for beryl using a transferable force field. *Am. Mineral.*, **82**, 1054-1062.

Salje, E. & Werneke, C. (1982): The phase equilibrium between sillimanite and andalusite as determined from lattice vibrations. *Contrib. Mineral. Petrol.*, **79**, 56-67.

Sherman, W.F. & Wilkinson, G.R. (1980): Raman and infrared studies of crystals at variable pressure and temperature. *In*: "Advances in Infrared and Raman Spectroscopy", Heyden, London, Vol. 6, p. 287-290.

Smirnov, M.B., Mirgorodsky, A.P., Quintard, P. (1995): CRYME: a program for simulating structural, vibrational, elastic, piezoelectric and dielectric properties of materials within a phenomenological model of their potential function. *J. Mol. Struc.*, **348**, 159-162.

Sykes, D. & Kubicki, J.D. (1996): Four-membered rings in silica and aluminosilicate glasses. *Am. Mineral.*, **81**, 265-272.

Wilkinson, G.R. (1973): Raman spectra of ionic, covalent and metallic crystals. *In*: "The Raman effect. Applications", (Anderson A, ed.), Vol. 2, Chapter 5. Dekker, New York.

Winkler, B. & Buehrer, W. (1990): Lattice dynamics of andalusite: prediction and experiment. *Phys. Chem. Minerals*, **17**, 453-463.

Winkler, B., Dove, M. T., Leslie, M. (1991): Static lattice energy minimization and lattice dynamics calculations on aluminosilicate minerals. *Am. Mineral.*, **76**, 313-331.

Received 15 June 2000
Modified version received 15 January 2001
Accepted 2 February 2001